EUROPEAN JOURNAL OF PURE AND APPLIED MATHEMATICS
2025, Vol. 18, Issue 1, Article Number 5773
ISSN 1307-5543 – ejpam.com
Published by New York Business Global

Maxwell Hybrid Nanofluid (Cu-Al_2O_3/Water) and (CuO-Ag/Water) Near a Stagnation Point above an Extending Sheet

Ahmed A. Gaber[1*], Mona A.A. Mohamed[2], Galal M. Moatimid[2]

[1] *Department of Mathematics, College of Science El-Zulfi, Majmaah University, Majmaah 11952, Saudi Arabia*
[2] *Department of Mathematics, Faculty of Education, Ain Shams University, Roxy, Cairo, Egypt*

Abstract. This article investigates Maxwell hybrid nanofluids (Cu-Al_2O_3/water and CuO-Ag/water) at a stagnation point over an extended sheet. The issue is motivated by its potential importance in enhancing thermal efficiency in modern heat transfer applications, crucial in optimizing manufacturing processes and energy conservation technology. Therefore, the present study investigates a non-Newtonian Maxwell nanoliquid across a mixed convection boundary layer (BL) and heat broadcast past a shrinking/stretching surface containing hybrid nanoparticles. In the current work, two different kinds of hybrid nanofluids are involved: Cu-Al_2O_3/water and CuO-Ag/water. Copper particles (Cu) and Copper oxide particles (CuO) are mixed into an Al_2O_3/water and Ag/water nanofluid to study these two types. The flow is acted upon the impact of a uniform magnetic field (MF) and a stagnation point. The issue arises from their enhanced thermal conductivity and heat transfer capabilities, which are crucial for enhancing energy efficiency in advanced cooling systems and engineering applications involving stagnation point flows. By utilizing suitable transformations, the partial differential equations (PDEs) are transformed into ordinary differential equations (ODEs). The prototype undergoes computational analysis utilizing the fourth-order Runge-Kutta (RK-4) method in conjunction with the shooting technique. The outcomes of the current work have applicable importance concerning the stagnation point flow, like cooling of nuclear reactors, cooling of microelectronic procedures by supporters, wire drawing, polymer extrusion, and many engineering hydrodynamic applications. The influences of the picked factors on the temperature, velocity, heat transmission rate, and skin friction factor are theoretically and numerically investigated. It is found that the existence of different hybrid nanoparticles with the influences of other parameters plays a significant role in both the velocity and temperature distributions. Additionally, the stagnation point creates a separation limit in the liquid flow that reverses the magnetic field influence between these flow regions.

2020 Mathematics Subject Classifications: 76A05, 76D10, 76W05, 80A20, 65L06
Key Words and Phrases: Hybrid nanofluid, Non-Newtonian Maxwell fluid, Stagnation point, Magnetohydrodynamics, Stretching surface

*Corresponding author.
DOI: https://doi.org/10.29020/nybg.ejpam.v18i1.5773

Email addresses: a.gaber@mu.edu.sa; aagaber6@gmail.com (A. A. Gaber), monaali@edu.asu.edu.eg (M. A.A. Mohamed), gal_moa@edu.asu.edu.eg (G. M. Moatimid)

Nomenclature

	English symbols		
u_i	Velocity components(m/s)	Ec	Eckert numeral
x_j	Model coordinates	R	Thermal radiation factor
f_i	Body force $(kg.m/c^2)$	μ_∞	Endless shear rate viscosity
k	Vortex viscosity coefficient $(kg/ms = N.s/m^2)$	T_∞	Temperature at infinity
T	Temperature of fluid$(Kelvin)$	q_r	Radiative heat flux
k_0	Relaxation time of the fluid		Greek symbols
B	Maxwell parameter	ρ	Fluid density(kg/m^2)
T_w	Temperature at wall	μ_{hnf}	Dynamic viscosity
k_{hnf}	Thermal conductivity$(S.m^{-1})$	$(\rho c)_f$	Heat capacity of the flow $(kg/m^3)(J.Kg^{-1}.K^{-1})$
R	Radiation factor	$(\rho c)_p$	Heat capability of the nanoparticles
Pr	Prandtl numeral	σ_{hnf}	Electrical conductivity
B_0	Uniform MF	ρ_{hnf}	Density conductivity
M	Magnetic parameter	v	Kinematic viscosity(m^2/s)

1. Introduction

The incorporation of nanoparticles is an effective method to enhance the thermal conductivity of practical fluids. Hybrid nanofluid is composed of two distinct nanoparticles suspended in various base fluids such as kerosene, water, and ethylene glycol. The thermal conductivity of hybrid fluids is significantly increased due to the presence of various nanoparticles in the base fluids, which enhances heat transfer mechanisms and reinforces applications in engineering and industry. The nanofluid, consisting of nanoparticles, was analyzed for heat transfer due to its enhanced thermal conductivity and several influencing parameters, including temperature, particle shape, and size [1]. Flat plate solar collectors and parabolic trough solar collectors are extensively utilized for home solar water heating applications. The impact of nanofluid on household solar water heating systems was examined [2]. The slip boundary condition and the dynamics of a rotating, three-dimensional, steady flow of nanoparticles over a flexible surface were described [3]. Two-phase notions of nanofluid were employed in physically existing models. A numerical and analytical model was created to examine heat transfer properties during machining and nanofluid lubrication [4]. The MF was applied perpendicular to the surface to safeguard the cutting material from fracture and excessive heating. An examination of entropy generation and thermal properties of a magnetic hybrid nanofluid, comprising silver and gold nanoparticles within the Eyring-Powell fluid, was conducted [5]. Heat exchangers are utilized in several applications, including chemical processes, power generation facilities, and air conditioning systems. The performance of these devices may be affected by various factors, including mass flow rates, stream temperatures, heat exchanger parameters, and

the thermo-physical properties of the fluid fluxes [6]. Instructions on the utilization of a boundary layer were supplied [7]. The effects of mass suction, Magnetohydrodynamics (MHD), Joule heating, viscous dissipation, and entropy formation were analyzed [8]. The numerical results indicated that the nanofluid's capacity for heat transmission, entropy generation, and flow was significantly influenced. Heat transmission in ternary nanofluids exhibits significant potential, especially in heat exchangers with parallel plates, as well as in chemical and applied thermal engineering. A study on the thermal increase between two parallel plates utilizing a ternary nanofluid was performed [9]. The model incorporates new insights into thermal radiation and modified Hamilton-crossers' thermal conductivity. The importance of sophisticated hybrid nanofluids is undeniable due to their diverse heat transfer applications. These are utilized not only in applied thermal, mechanical, and chemical engineering but also serve as coolants for nuclear reactors, in paint, medical sciences, and the production of numerous household items. A dynamical analysis of fluid properties within a conduit featuring gradually expanding or contracting walls was documented [10].

The BL flow across a stretching sheet has garnered significant attention due to its many applications in manufacturing processes, such as polymer extrusion from a die chemical catalytic reactors and geothermal reservoirs. The fluid motion in proximity to a solid surface's stagnation region is termed stagnation point flow. Stagnation points are evident in various application domains, including submarines, aircraft, and flows over rocket tips. The issue of stagnation point flow is explored through several methodologies, including boundary layer analysis. The free convective flow of a non-Newtonian nanofluid produced by a spinning stretchable disc was examined [11]. The study analyzed the Stefan blowing Cattaneo–Christov with mass and heat fluxes as a definitive illustrative model. A non-Newtonian MHD Carreau nanofluid over a stretched vertical cylinder within incompressible BL containing mobile microorganisms was documented [12]. The flow occurs in permeable media and according to the modified Darcy's law. The system was saturated by an unaltered normal magnetic strength to the walls. The movement of a boundary layer in an incompressible non-Newtonian Williamson nanofluid was illustrated [13]. The BL was situated near a vertically orientated, porous surface that was undergoing exponential stretching. Motile microorganisms were implicated in movement through a permeable media, in accordance with the modified Darcy's law. A study was conducted on the slip bioconvective movement of a non-Newtonian Sutterby nanofluid layer containing motile microorganisms, with the fluid layer flowing over a curved stretched surface [14]. The bioconvection dynamics of an incompressible non-Newtonian Sutterby liquid on a deformable surface, incorporating both nanomaterial and microorganisms, were examined [15]. The liquid traverses a permeable area and is influenced by a uniform vertical MF. The issue of stagnation point flow in carbon nanotubes, influenced by suction/injection effects on a stretching/shrinking sheet, was investigated [16]. A thorough examination of the boundary layer flow and heat transfer study of the stagnation point flow of pair stress fluid across an exponentially stretched surface was conducted [17]. The governing equations of the pair stress fluid model were derived using the BL technique. The stagnation point of incoming flow impacting a stretchy flat plate or a circular cylinder was investigated [18].

Precise solutions are sought for both momentum and heat fields. The identified analytical solutions are crucial as they provide more exact solutions to the Navier–Stokes and energy equations. The distinctive properties of nanofluid were prominently highlighted due to the identification of enhanced thermal efficiency [19]. Consequently, the focus was on the laminar boundary layer of axisymmetric stagnation point flow of Casson nanofluid across a stretched plate or cylinder, influenced by thermal radiation and suction/injection. The numerical dual solution of stagnation point flow and melting heat transfer of Casson fluid induced by a stretching sheet was investigated [20].

Magnetohydrodynamics (MHD) refers to the behavior of a fluid influenced by electromagnetic fields, contingent upon its adequate electrical conductivity. The MHD is a technique employed in energy harvesting to generate electricity directly from the movement of conducting fluids. The electric energy recovery method in these applications is contingent upon the types of utilized fluids, primarily ionic plasma (hot gases), liquid metals, and saline solutions. They may also be mounted on the chimneys of enterprises that emit hot gases as waste, in power plants where such setups are integrated with gas or steam turbines, and in heating, ventilation, and air conditioning systems where hot gases circulate [21-23]. Seawater, owing to its prevalence and application in numerous industrial sectors, is regarded as a compelling conductive fluid, hence motivating researchers to pursue optimal utilization of its diverse physical phenomena [24, 25]. Research concerning the extraction of MHD energy from seawater can be categorized into three primary axes based on installation location: the first involves deployment near the shore or in the open ocean to capture wave energy; the second entails seabed installations for wave energy recovery; and the third consists of installations on mobile vessels [26]. A proposal for an MHD energy recovery module for a seawater desalination facility utilizing reverse osmosis technology has been presented. The motile microorganisms in an MHD flow of an incompressible nanofluid adhering to the non-Newtonian Jeffrey model were investigated [27]. This may be advantageous for microorganisms and many applications. The structure was affected by a homogeneous MF perpendicular to the discs, accounting for the Hall Effect. The bioconvection dynamics of an incompressible non-Newtonian Sutterby liquid on a deformable surface, incorporating both nanomaterial and microorganisms, was investigated [28]. The liquid traverses a permeable area and is influenced by a uniform vertical MF. The inner spine of a relativistic jet was analyzed to determine the bulk acceleration and the jet's morphology, as well as to comprehend how these parameters are influenced by enthalpy and MF strength [29]. A proficient method for determining the ideal decay estimates for solutions of the 3D anisotropic MHD equations with solely horizontal dissipation was documented [30]. A numerical analysis was conducted on steady mixed convection in a two-dimensional enclosure filled with Cu/H2O nanoliquid through a porous media [31]. The influence of a magnetic dipole on a nonlinear thermally radiative ferromagnetic liquid flowing across a stretched surface, considering Brownian motion and thermophoresis, was examined [32].

Maxwell hybrid nanofluids, including Cu-Al_2O_3/water and CuO-Ag/water, exhibit considerable potential for improving heat transfer processes owing to their combined thermal properties and distinct rheological characteristics. These fluids, consisting of metal

and metal oxide nanoparticles dispersed in a base fluid such as water, are especially efficient in applications necessitating elevated thermal conductivity and consistent performance under harsh temperatures. Near a stagnation point above an extending sheet, the flow and heat transfer characteristics are significantly affected by the interaction between the fluid and the boundary layer. Experimental and theoretical investigations indicate that Maxwell hybrid nanofluids exhibit enhanced heat dissipation properties, rendering them suitable for sophisticated cooling systems in sectors such as aerospace, electronics, and renewable energy. In the design of heat exchangers, the improved thermal conductivity of Cu-Al_2O_3/water or CuO-Ag/water facilitates more efficient energy transfer, hence decreasing the overall system size and cost. Moreover, these fluids are utilized in the thermal management of high-powered microchips, where localized heat hotspots may be efficiently regulated due to their superior thermal diffusion properties. In renewable energy systems, such as solar collectors, these nanofluids enhance the efficiency of heat absorption and transfer. The stale point flow configuration across an expanding sheet simulates real-world situations in aerodynamic heating or turbine blade cooling, where hybrid nanofluids contribute to thermal stability and operational efficiency. The Maxwell viscoelastic behavior offers insights into the dynamic response of these fluids, facilitating optimization in systems that necessitate precise control over fluid characteristics and energy dissipation rates. Therefore, the current work is based on the aforementioned motivating aspects besides the industrial and engineering significance of hybrid nanofluids in improving heat flow transference. A system of common nonlinear PDEs is generated from the main equations of motion, which is converted to another ODE one utilizing proper transformations. The RK-4 procedure with the shooting technique is employed here to scrutinize this system numerically. The major conceptions of this problem can be outlined to answer some significant queries:

i. How does the movement of a non-Newtonian Maxwell liquid including hybrid nanoparticles occur in a border layer across a stretched plate?

ii. How do the structured distributions operate with the existence of Al_2O_3-Cu or, Ag-CuO particles?

iii. What is the impact of the existence of a stagnation point on the flow distributions?

iv. How do the uniform normal magnetic strength, Ohmic dissipation, and radiation affect the flow and the related gatherings of particles?

In order to follow the paper easily, the manuscript is constructed as follows: In § 2 and its subsections 2.1 and 2.2, the prototype structure, fundamental equations, applicable boundary conditions, and the related physical aspects are examined. The proper non-dimensional forms that convert the principal dimensional PDEs into dimensionless ones are illustrated in subsection 2.3. In § 3, some details of the numerical methodology of the solution are described. In § 4, the outcomes and their physical explanations, are sketched. Finally, the conclusion is outlined in § 5.

2. Prototype Construction

The formulation of Maxwell hybrid nanofluids, including Cu-Al_2O_3/water and CuO-Ag/water, at a stagnation point above an extending sheet, entails the examination of fluid flow and heat transmission properties influenced by hybrid nanoparticles floating in a base fluid. These nanofluids are formulated by distributing two categories of nanoparticles (e.g., copper (Cu) and aluminum oxide (Al_2O_3) in the first instance, and copper oxide (CuO) and silver (Ag) in the second) within water as the base fluid. The governing equations are formulated from the continuity, momentum, and energy equations, adjusted to incorporate the influences of nanoparticle volume fractions, thermal conductivity, and dynamic viscosity of the hybrid nanofluid. The BL equations consider the velocity profile of the stretching or extending sheet, with boundary conditions at the surface comprising the no-slip requirement for velocity and specified temperature or heat flux at the sheet. For hybrid nanofluids, thermo physical parameters including density, heat capacity, thermal conductivity, and viscosity are determined using weighted averages of the properties of the base fluid and the individual nanoparticles. Maxwell's model enhances heat transfer analysis by including effective thermal conductivity, accounting for the synergistic effects of scattered nanoparticles. The stagnation point flow presumes a stable, two-dimensional incompressible fluid, characterized by equilibrium between the velocity of the stretching sheet and the impinging flow. Dimensionless similarity variables are utilized to convert partial differential equations into a system of ordinary differential equations, which are subsequently solved either numerically or analytically to examine the effects of parameters including nanoparticle volume fraction, stretching ratio, Prandtl number, and thermal conductivity ratio on velocity and temperature profiles. The current model demonstrates a non-Newtonian laminar hydrodynamic two-dimensional hybrid nanofluid flow in the region of an expanding surface and follows Maxwell's prototype [31]. The novelty of this work arises from modeling the flow of Maxwell's fluid with classifying hybrid nanoparticle distributions across an extending layer. The Cartesian coordinate model is utilized, where the stretching border is horizontally associated with the x-axis, and the y-axis is directed normally to the plate as shown in the sketching model Fig. 1. Consequently, the elongating plane is situated at $y = 0$, which springs along with the x-direction with a uniform stretching parameter. The movement is presumed to be limited by the boundary layer area $y > 0$ with a fixed stagnation point located at $x = 0$. The stretching speed $U_w(x)$ and the ambient speed $U_e(x)$ are chosen to linearly vary from the inactivity point, where $U_w(x) = cx$ and $U_e(x) = ax$. The sheet is maintained at a fixed heat T_w, further, as tends to infinity, heat approaches T_∞. Under this preparation, the flow addresses itself to the velocity and heat slip at the surface. In combination with the vertical axis of the stretching sheet, an MF of uniform strength intensity B_0 is exposed. For the sake of simplicity, the involvement of an electric induction may be ignored. The absence of the induced magnetic intensity is owing to the supposition of a small Reynolds numeral [32] and [33]. The existence of the Lorenz force causes magnetization of the fluid. One of the furthermost significant implications of our prototype is the flow over the stretching sheet in the parabolic solar collector channel which is a part of solar cell systems like solar aircraft

wings, solar water pumps, ...etc. Jamshed et al. [34] and [35] observed that the usage of nanofluids and hybrid nanofluids enhanced the thermal transfer, and hence enriched the effectiveness of the solar cell. The relationship between our model and this real application is that the current flow is studied on a stretching sheet utilizing hybrid nanoparticles such as Jamshed suggested. Additionally, the assumed fluid is non-Newtonian under the belongings of the magnetic field, Ohmic dissipation, and thermal radiation, which are considered promising properties within the aforementioned applications.

D'Alembert [36] first presented the fluidic stagnation point concept based on the principle of movement drag on solid limitations. Two centuries later, Prandtl [37] planned the BL concept. Taylor [38] demonstrated the systematic implication of trapping matters with fluidic stagnation point flows. Stagnation point flow is highly relevant in applications involving heat transfer and fluid dynamics near boundaries with localized forces or heat sources.

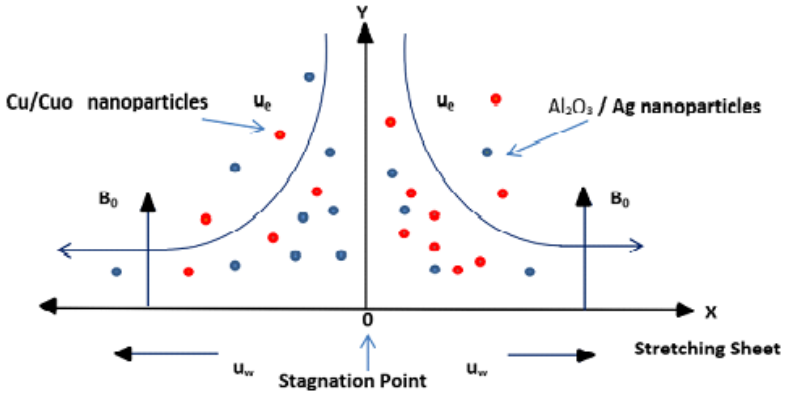

Fig. 1: Sketch of the flow construction model.

2.1. The Fundamental Equations of Motion

The fundamental equations may be formulated as [39-41]:

$$\frac{\partial u}{\partial x}+\frac{\partial u}{\partial y}=0, \tag{1}$$

and

$$u\frac{\partial u}{\partial x}+\upsilon\frac{\partial u}{\partial y}=U_e\frac{\partial U_e}{\partial x}+\frac{\mu_{hnf}}{\rho_{hnf}}\frac{\partial^2 u}{\partial y^2}+\frac{\sigma_{hnf}B_0^2}{\rho_{hnf}}(U-u)-k_0(u^2\frac{\partial^2 u}{\partial x^2}+\upsilon^2\frac{\partial^2 u}{\partial y^2}+2u\upsilon\frac{\partial^2 u}{\partial y\partial x}) \tag{2}$$

The energy and the nanoparticle are previously specified [42] as:

$$u\frac{\partial T}{\partial x}+\upsilon\frac{\partial T}{\partial y}=\frac{k_{hnf}}{(\rho c_p)_{hnf}}\frac{\partial^2 T}{\partial y^2}+\sigma_{hnf}\frac{B_0^2}{(\rho c)_f}u^2-\frac{1}{(\rho c)_f}\frac{\partial q_r}{\partial y} \tag{3}$$

As previously shown [43], the radiative temperature flux may be expressed as:

$$q_r = \frac{-4\sigma^*}{3k_R}\frac{\partial T^4}{\partial y}. \tag{4}$$

It should be noted that the current work assumes slip velocity and thermal nanoparticles at the surface wall. Therefore, the appropriate border conditions may be formulated as:

$$\left.\begin{array}{c} u = U_w(x) = cx, \upsilon = 0, \, T = T_w, \quad at \;\; y = 0 \\ u \to U_e(x) = ax, \upsilon \to 0, \;\; , T \to T_\infty \;\; as \;\;\; y \to \infty \end{array}\right\}, \tag{5}$$

where a and c are constants, cx is the velocity at the wall, $ax$is the velocity far from the wall, and $T_w > T_\infty$. Moreover, Table 1 represents the physical characteristics of any hybrid nanofluid, which are included in the equation of motion (2) and the energy equation (3). Table 2 also indicates the values of these properties in the situation of Al_2O_3-Cu-water and CuO-Ag-water hybrid nanofluids.

Table 1:

Thermophysical features of hybrid nanofluid

Property	Hybrid nanofluid
Density	ρ_{hnf}=$(1-\varphi_1)((1-\varphi_1)\rho_f + \varphi_1\rho_{s1}) + \varphi_2\rho_{s2}$
Heat capacity	$(\rho c_p)_{hnf}$=$(1-\varphi_1)((1-\varphi_1)(\rho c_p)_f + \varphi_1(\rho c_p)_{s1}) + \varphi_2(\rho c_p)_{s2}$
Dynamic viscosity	$\mu_{hnf} = \frac{\mu_f}{(1-\varphi_1)^{2.5}+(1-\varphi_2)^{2.5}}$
Thermal conductivity	$\frac{k_{hnf}}{k_{nf}} = \frac{k_{s_2}+2k_{nf}-2\varphi_2(k_{nf}-k_{s_2})}{k_{s_2}+2k_{nf}+\varphi_2(k_{nf}-k_{s_2})}$, where $\frac{k_{nf}}{k_f} = \frac{k_{s_1}+2k_f-2\varphi_1(k_f-k_{s_1})}{k_{s_1}+2k_f+\varphi_1(k_f-k_{s_1})}$
Electrical conductivity	$\frac{\sigma_{hnf}}{\sigma_{nf}} = \frac{\sigma_{s_2}+2\sigma_{nf}-2\varphi_2(\sigma_{nf}-\sigma_{s2})}{\sigma_{s2}+2\sigma_{nf}+\varphi_2(\sigma_{nf}-\sigma_{s2})}$, where $\frac{\sigma_{nf}}{\sigma_f} = \frac{\sigma_{s_1}+2\sigma_f-2\varphi_1(\sigma_f-\sigma_{s_1})}{\sigma_{s_1}+2\sigma_f+\varphi_1(\sigma_f-\sigma_{s_1})}$

Table 2:

Thermophysical characteristics of water and Al_2O_3, Cu, CuO, and Ag nanoparticles

Physical property	Fluid phase (water)	$Al_2O_3\,\varphi_1$	Cu φ_2	CuO φ_1	Ag φ_2
$\rho/(\mathrm{kgm}^3)$	997.1	3 970	8 933	6500	10500
$C_p/(\mathrm{J.Kg}^{-1}.\mathrm{K}^{-1})$	4 179	765	385	535.6	235
$k/(\mathrm{W.m}^{-1}.\mathrm{K}^{-1})$	0.613	40	400	20	429
$\sigma/(\mathrm{S.m}^{-1})$	0.05	3.69×10^7	5.96×10^7	5.96×107	3×106

2.2. Important Physical Quantities

The significant physical amounts in this analysis are the skin friction parameter**,** Cf_y which acts along the y direction, and the Nusselt numeral Nu. They are described as:

$$Cf_y = \frac{\tau_w}{\rho(ax)^2}, \;\; \tau_\omega = \left(\frac{\partial u}{\partial y}\right)_{y=0}, \tag{6}$$

where the skin friction parameter indicates the local amount and substantially it implies the ratio between the local shear stress to the dynamics pressure, where

$$Nu = \frac{xq_w}{k\left(T_w - T_\infty\right)}, \;\; q_w = -k\left(\frac{\partial T}{\partial y}\right)_{y=0}, \tag{7}$$

represents the Nusselt numeral that is addressed as the ratio between convective and conductive temperature transmission.

2.3. Convenient Conversions of Relationship

The fundamental nonlinear PDEs are transformed into alternative ordinary ODEs by an effective similarity conversion. Drawing on the work of [44] and [45], the required similarity transformations can be created as:

$$\left.\begin{array}{ll} u = U_e f'(\eta) = axf'(\eta), & \upsilon = -\sqrt{a\nu_f} f(\eta), \\ \theta(\eta) = \frac{T-T_\infty}{T_w - T_\infty}, & \text{and } \eta = \sqrt{\frac{a}{\nu_f}} y \end{array}\right\}, \tag{8}$$

where $f(\eta)$ and $\theta(\eta)$ are non-dimensional speed and heat, correspondingly, and η is a non-dimensional relationship coordinate.
Under the conversions (8), Eqs. (1-3) may be formulated as:

$$\frac{\mu_{hnf}/\mu_f}{\rho_{hnf}/\rho_f} f''' + ff'' - \left(f'\right)^2 + M^2 \frac{\sigma_{hnf}/\sigma_f}{\rho_{hnf}/\rho_f}\left(1 - f'\right) - Bf^2 f''' + 2Bff'f'' + 1 = 0, \tag{9}$$

$$\frac{1}{\Pr}\left(\frac{1}{(\rho c_p)_{hnf}/(\rho c_p)_f}\right)\left(\frac{k_{hnf}}{k_f} + \frac{4}{3}R\right)\theta'' + f\theta' + \frac{\sigma_{hnf}/\sigma_f}{(\rho c_p)_{hnf}/(\rho c_p)_f} M^2 Ecf'^2\theta = 0, \tag{10}$$

The solutions of these equations are subjected to the border restrictions:

$$\left.\begin{array}{lll} f' = A,\; f = \mathrm{s},\; \theta = 1, & \text{at} & \eta = 0 \\ f' = 1,\; \theta = 0 & \text{as} & \eta \to \infty \end{array}\right\} \tag{11}$$

where

$$M^2 = \frac{\sigma_f B_0^2(x)}{a\rho_f}, Ec = \frac{\alpha U_w}{a(c_p)_f}, B = k_0 a, \Pr = \frac{\upsilon_f}{\alpha_f}, Ec = \frac{\alpha U_w}{a(c_p)_f}, R = \frac{4\sigma^* T_\infty^3}{k_f k^*}, A = \frac{c}{a}, \tag{12}$$

3. Numerical Technique

In the current calculation, the fundamental nonlinear equations PDEs are converted, as previously seen, to ODEs with appropriate transformations. The nonlinear ODEs, as shown in Eqs. (9) and (10), are subjected to the convenient BCs. As given in Eqs. (11), they are structured by the shooting technique by the subroutine D02HAF of the NAG Fortran library [46]. D02HAF illustrates the two-point boundary-value problem for the construction of ODE, by the RK-4 method with Newtonian iteration in conjunction with

the shooting and similar procedures [47]. The fourth-order Runge-Kutta method (RK4) is a broadly used numerical method for solving ordinary differential equations (ODEs). It is mainly significant because of its balance between accuracy and computational effectiveness. It has many advantages, where it performs effectively on a wide range of problems, including those with moderate non-linearity or smooth solutions. This technique is frequently applied to beginning value and boundary value problems in physics, engineering, and other fields. This approach is operating now with the help of Mathematica Software. The procedure stays in reiteration until convergence is attained. One of the most dependable and adaptable numerical techniques for resolving ordinary differential equations (ODEs) is the Runge-Kutta 4th Order Method (RK4). When compared to alternative numerical techniques, its benefits include:

1. **Accuracy**
   Fourth-order accuracy is attained by RK4, which means that its global error falls in proportion to h4 (where h is the step size). For the same step size, this is substantially more accurate than lower-order techniques like the Midpoint method (second-order) or the Euler method (first-order).

2. **Consistency**
   Particularly for stiff or sensitive issues, RK4 is more stable than more straightforward techniques like Euler's approach. It can manage more complicated dynamics without experiencing instability because of its increased precision at every step.

3. **Effectiveness**
   Even though RK4 needs more calculations per step than second-order or Euler techniques, its increased accuracy frequently permits bigger step sizes, which lowers the overall number of steps and increases efficiency.

4. **Harmony between accuracy and Complexity**
   Unlike higher-order or specialized methods (e.g., implicit methods), RK4 is reasonably simple to implement and does not need sophisticated derivations. It offers a nice balance between accuracy and computing complexity.

5. **Generality**
   RK4 may be used to solve a variety of issues without the need for adjustments. It is capable of efficiently managing non-linearity issues and ODE systems.

6. **Error Control**
   In non-adaptive implementations, frequent step size modifications are less necessary because RK4 by default offers a modest truncation error for each step.

Furthermore, The limits of the RK-4 technique are summarized in:

i. It needs an initial guess of the higher order of the targeted functions.

ii. It uses a fixed step size.

iii. Four function evaluations are required for each step.

iv. It has a low truncation error per step.

To begin this procedure, Eqs. (9) and (10) could be rewritten as:

$$f''' = \frac{-\rho_{hnf}/\rho_f}{(\mu_{hnf}/\mu_f - (\rho_{hnf}/\rho_f)Bf^2)}\left(ff'' - (f')^2 + M^2\frac{\sigma_{hnf}/\sigma_f}{\rho_{hnf}/\rho_f}(1-f') + 2Bff'f'' + 1\right), \tag{13}$$

$$\theta'' = \left(\frac{-\Pr(\rho c_p)_{hnf}}{(\rho c_p)_f\left(\frac{k_{hnf}}{k_f} + \frac{4}{3}R\right)}\right)\left(f\theta' + \frac{\sigma_{hnf}/\sigma_f}{(\rho c_p)_{hnf}/(\rho c_p)_f}M^2 Ecf'^2\theta\right). \tag{14}$$

The configuration can be expressed by considering the following assumptions:

$$f = y_1,\ \ \mathrm{y}_1' = y_2, \mathrm{y}_2' = y_3, \theta = y_4,\ \text{and}\ \theta' = y_5, \tag{15}$$

Eqs. (13) and (14) then become:

$$\left.\begin{aligned} \mathrm{y}_3' &= \tfrac{-\rho_{hnf}/\rho_f}{(\mu_{hnf}/\mu_f - (\rho_{hnf}/\rho_f)By_1{}^2)}(y_1\, y_3 - (y_2)^2 + M^2\tfrac{\sigma_{hnf}/\sigma_f}{\rho_{hnf}/\rho_f}(1-y_2) + 2By_1y_2y_3 + 1), \\ y_5' &= -\left(\tfrac{\Pr((\rho c_p)_{hnf})}{(\rho c_p)_f(\frac{k_{hnf}}{k_f}+\frac{4}{3}R)}\right)\left(y_1\, y_5 + \tfrac{\sigma_{hnf}/\sigma_f}{(\rho c_p)_{hnf}/(\rho c_p)_f}M^2 Ec\, y_1{}^2 y_4\right) \end{aligned}\right\} \tag{16}$$

Then, this system of ODEs can be solved in accordance with the initial conditions:

$$f(0) = A,\ \ y_1(0) = 1,\ \ \theta(0) = 1 \tag{17}$$

Since these conditions are not adequate to catch the solutions of Eqs. (16), a primary guess for $y_3(0)$, $y_5(0)$ is carefully chosen before starting the solving procedure. Initially, the solutions start in the locality of $\eta = 10^{-4}$ to avoid the singularity at $\eta = 0$. The RK-4 method is employed with the aid of Mathematica Software, and the solutions are realized numerically. The obtained solutions converge when the residuals (the differences between the reachable and indomitable values) of $y_2(\infty)$, $y_4(\infty)$ are less than 10^{-6}, where infinity is considered as $\eta_\infty = 6$. If the reached solution does not match the convergence limit, then the initial guesses are re-formulated by Newton's procedure, and the process is continued until the solution matches the required convergence [47]. Contrary to the classical RK-4, the novel approach uses only two memorial positions per dependent variable, which is easier and more precise than the standard scheme. This methodology is significant for displaying linear wave phenomena.

4. Outcomes and Interpretations

Heat transfer and fluid dynamics may be advanced in a variety of engineering and industrial applications by using hybrid non-Newtonian nanofluids in stagnation point flows over shrinking/stretching surfaces. These fluids maximize thermal management in systems where high accuracy and efficiency are crucial by utilizing their optimized viscosity

profiles and improved thermal conductivity. The current work illustrates the flow of an incompressible non-Newtonian hybrid nano liquid comprising two hybrid nanoparticles: Al2O3-Cu and CuO–Ag. The fluid obeys a non-Newtonian Maxwell model, and the flow is induced by a regular normal magnetic field taking into account the stagnation point effect. The temperature distribution is studied with the Joule heating and thermal radiation influences. The mathematical construction is concerned with momentum and energy equations along with different coefficients of the hybrid nanoparticles under linear conditions of the stretching slip velocities. The current section illustrates the effects of the various factors on the flow speed, heat diffusion, skin friction, and Nusselt coefficients. Various graphs are schemed to reach the physical explanations of the concluded outcomes. In what follows, specific values of the relevant parameters are considered when drawing the profiles which diverge according to the deliberate factor in each graph.

Velocity Distributions

Figs. 2-9 indicate the speed profiles $f'(\eta)$ vs the dimensionless factor η. These graphs are calculated to study the effects of the slip factor on the stagnation point A, the magnetism coefficient M, the viscoelasticity factor$B$, and the volume fraction coefficients $\phi_1$and ϕ_2 on $f'(\eta)$for the two discussed hybrid nanofluids Cu-Al_2O_3-water and CuO-Ag-water.

Figs. 2 and 3 show that the speed f' slightly grows with the growth of the magnetic coefficient M as $A > 1$, while it strongly decreases with M as $A < 1$. Physically, the growth of M is supplemented by the improvement of the Lorentz force which grounds a delay in the flow and then reduces the flow velocity. These outcomes have been previously reported [48]. The magnetic coefficient alters heat transfer rates, boundary layer thickness, and velocity profiles, which have a substantial impact on stagnation point flows. These effects are especially noticeable in hybrid non-Newtonian nanofluids because of the interaction of magnetic fields with temperature and rheological characteristics. The dampening effect of the magnetic field causes the fluid velocity close to the sheet to drop as M rises. A thicker momentum barrier layer results from this. Applications in industrial, aeronautical, and energy sectors can improve performance and control by utilizing these interactions.

Figs. 4 and 5 show that the speed f' improves with the growth of B. Actually, the growth of the viscoelasticity factor Bmaterially leads to a growth in the fluid viscosity, but it seems that the existence of the hybrid particles works to weaken this viscosity and hence raises the speed. This result agrees with that of [49] and [50]. Increased viscoelasticity prevents deformation by adding elasticity effects to the fluid. As a result, the fluid motion slows down and the velocity gradient close to the stagnation point decreases. In contrast to strictly viscous fluids, viscoelastic fluids have a delayed reaction to the applied stress at the stagnation point, resulting in altered velocity profiles. In the stagnation area, this frequently reduces the flow rate. When the viscoelastic parameter is increased, the velocity in the boundary layer tends to increase around the stagnation point or in streams close to an extending sheet. The fluid's ability to adapt its flow behavior to surface stretching or deformation is facilitated by its elasticity. As a result, the velocity is higher close to the wall.

Figs. 6 and 7 examine the influence of the stagnation point on the speed $f'(\eta)$. As one can see from these figures, the velocity increases at the two sides of the stagnation point

with the increase of the slip constant A. The velocity distribution of the fluid as it gets closer to the point where the velocity is zero (the stagnation point) is referred to as the flow velocity near the stagnation point. The fluid is drawn toward a point on the surface (like an extended sheet) in stagnation point flow when the flow velocity drops to zero. The rise of A postulates that the ratio concerning the speed at the wall and the ambient speed gets bigger. Thus, it is logical that when the border speed rises, the speed of the flow rises. This outcome is significant in most applications that consider the boundary layers' flow rates. The influences of the volume fraction coefficients ϕ_1 and ϕ_2 are illustrated through Figs. 8 and 9. Due to the similarity of the effect of ϕ_1 and ϕ_2 in the two cases, one case is presented for each parameter for reasons of space. It is seen from Fig. 8 that the speed rises with the rise of ϕ_1 which represents the Al_2O_3 or CuO particle concentration. The addition of nanoparticles (e.g., Cu, Al_2O_3) develops the heat transfer capacity of the fluid, which can decrease the thickness of the thermal boundary layer and enhance the velocity. However, More flow resistance results from the inclusion of nanoparticles like CuO or Ag, which increase the fluid's viscosity. Resistance rises and flow velocity decreases as the concentration of nanoparticles increases because of the increased contact between the nanoparticles and the fluid. Therefore, it is revealed that the speed decreases with the increase of ϕ_2 which signifies the Cu or Ag particle concentration, as seen from Fig. 9.

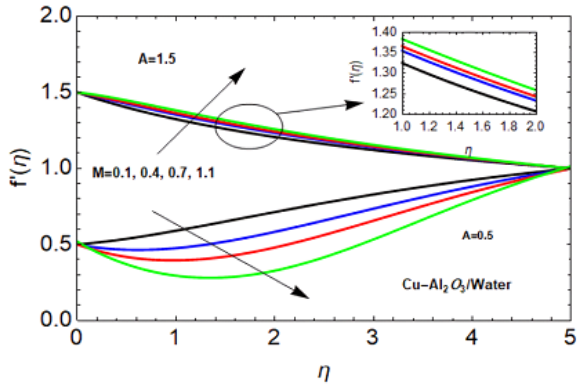

Fig. 2: Speed profile $f'(\eta)$ against η to show the influence of the magnetic factor M on the stagnation point in the case of Cu-Al_2O_3-water.

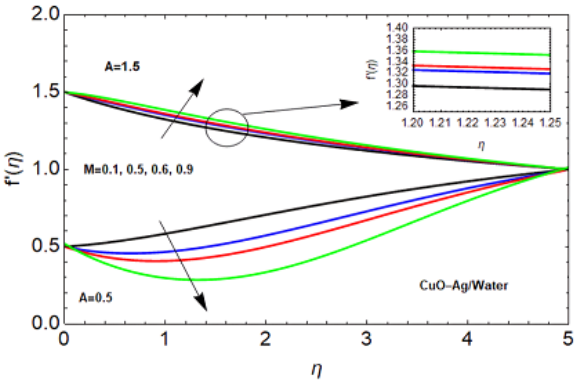

Fig. 3: Speed profile $f'(\eta)$ against η to show the influence of the magnetic factor M on the stagnation point in the case of CuO-Ag-water.

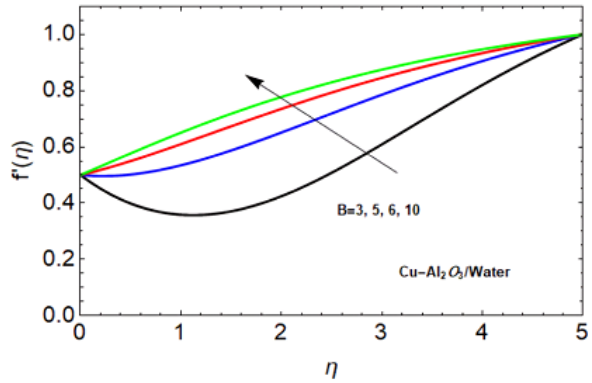

Fig. 4: Speed profile $f'(\eta)$ against η to display the influence of the viscoelastic factor B in the case of Cu-Al_2O_3-water.

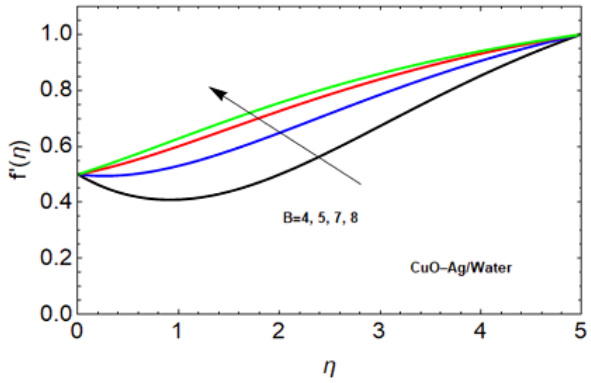

Fig. 5: Speed profile $f'(\eta)$ against η to display the influence of the viscoelastic factor B in the case of CuO-Ag-water.

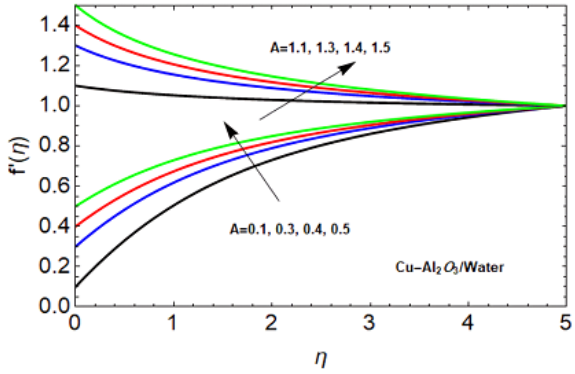

Fig. 6: Speed profile $f'(\eta)$ against η to show the influence of the slip factor A on the stagnation point in the case of Cu-Al_2O_3-water.

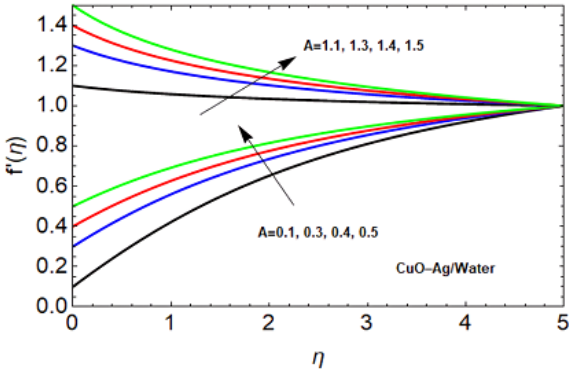

Fig. 7: Speed profile $f'(\eta)$ against η to show the influence of the slip factor A on the stagnation point in the case of CuO-Ag-water.

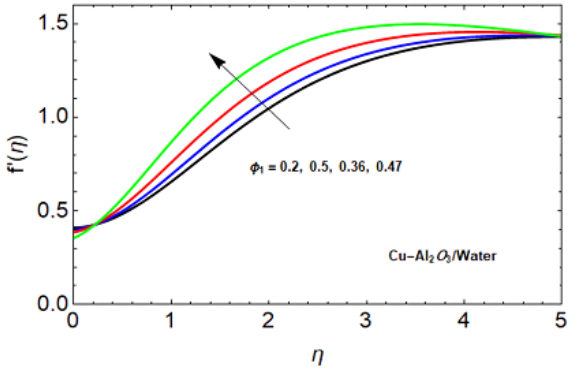

Fig. 8: Speed profile $f'(\eta)$ against η to display the influence of the Al_2O_3 or CuO nanoparticles concentration ϕ_1.

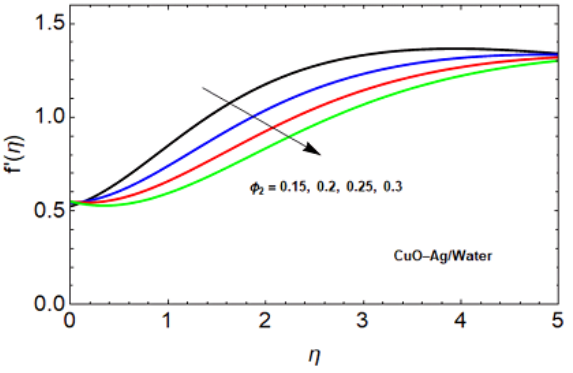

Fig. 9: Speed profile $f'(\eta)$ against η to display the influence of the Cu or Ag nanoparticles concentration ϕ_2.

Temperature Profile

Heat transfer is one of the actual necessary features to examine the flows of fluids, particularly those connected to hybrid nanofluids. Figs. 10-21 represent the heat profile θ versus the non-dimensional factor η, in the two illustrated cases of hybrid nanofluids, to exemplify the influences of the Eckert numeralEc, the magnetism coefficient M, the Prandtl numeral Pr , the radiation coefficient R, the viscoelasticity factor B, the nanoparticles volume fractions φ_1, and φ_2.

It is observed that the growth of the Eckert numeral Ec raises θ as showed by Figs. 10 and 11. Physically, the Eckert numeral Ec denotes the physical connection between the movement kinetic energy and the boundary surface enthalpy variation; it also defines heat diffusion dissipation. This temperature dissipation produces temperature due to the interaction of the connecting fluid particles. This collaboration between particles improves with the existence of those hybrid nanoparticles, which leads to an improvement in the elementary liquid temperature. These outcomes agree with the previously obtained outcomes [50]. A high Eckert Number means that kinetic energy is significantly converted to thermal energy by viscous dissipation, raising the fluid's temperature close to the stagnation point. Additionally, due to the dissipation-induced temperature rise, the temperature gradient at the surface is reduced, which lowers the heat transfer rate to the surface. Furthermore, Higher Eckert numbers result in increased fluid velocity, which enhances heat transfer by transferring more energy between the fluid and the surface.This is due to the fact that higher fluid mixing and improved convective heat transfer from the surface to the bulk fluid are caused by faster fluid flow.

Figs. 12 and 13 show the effect of the magnetism coefficient M on θ. From these figures, it is obvious that the heat energy rises with the increase of M. As previously mentioned, the growth of the magnetism coefficient promotes the Lorentz force, which in turn gives rise to a slow stream and growth in the heat transfer, as attained in Figs. 3 and 8. This consequence signals that the performance of an MF shows a significant role in enhancing thermal convection in most applications. In certain situations, the fluid's capacity to mix may be diminished by the increased magnetic field, which might result in localized temperature rises close to the stagnation point or surface because of less convective cooling. Moreover, because convective heat transmission is suppressed as the magnetic parameter rises, localized temperature increases, particularly close to the surface, which may result from less fluid mobility and thicker boundary layers. This result is consistent with the mainstream research in this field [48] and [51].

The impact of the Prandtl numeral Pr on θ is examined by Figs. 14 and 15. It is shown that the growth of the Prandtl numeral Pr reduces heat transmission. Prandtl numeral indicates the ratio concerning the thickness of the momentum diffusivity layer and that of the thermal diffusivity layer. The rate of heat transmission from the fluid's surface decreases as Pr rises because the thermal boundary layer thickens. Because heat is not effectively transmitted away from the wall, temperatures are lower close to the surface. Additionally, The temperature gradient in the thermal boundary layer tends to be steeper close to the surface when the Prandtl number is larger, which causes the temperature to drop farther away. Accordingly, the rise of Pr indicates low thermal conductivity and low-

temperature dispersion, which is confirmed in Figs. 14 and 15. This outcome is consistent with that of [33] and [49].

Furthermore, Figs. 16 and 17 demonstrate the influence of the radiation limitation R on heat transmission θ. It is shown that heat advances with the rise of R in the two cases. Physically, the radiation factor R represents the proportion of thermal transfer by conduction to thermal transmission by radiation. Also, it is observed that the rise in radiation parameter R enhances the thickness of the thermal BL; therefore, fluid temperature grows owing to the occurrence of extraordinary radiation in the movement field. In contrast to conductive or convective heat transfer, radiative heat transfer becomes increasingly important as the radiation parameter rises. The fluid's temperature rises as a result, particularly close to the surface. Moreover, The thermal boundary layer thickens as a result of the increased radiation. This occurs because radiation raises the temperature of the fluid close to the surface by directly transferring heat from the surface to the fluid. This outcome is in good agreement with the previously obtained findings [52]. Figs. 18 and 19 illustrate the influence of the viscoelasticity factor B on θ. It is also found that the temperature increases with the rise of B in the case of Al_2O_3-Cu dissolved particles, whereas B approximately has no effect in the case of CuO-Ag particles. The growth of the viscoelasticity factor B materially leads to a development in the fluid viscosity, which means a relaxed motion and an improvement in the flow temperature. Physically, The fluid shows increasing internal friction and flow resistance as the viscoelastic parameter rises, which causes viscous dissipation to generate more heat inside the fluid and the fluid may heat up as a result. Also, the thicker thermal boundary layer caused by the higher viscosity and elastic behavior lowers the heat transmission efficiency. Nevertheless, the fluid's temperature tends to rise due to internal friction and viscous dissipation, especially close to the surface. This conclusion agrees with [50] and [51].

Figs. 20 and 21 are a graphical representation of the impact of the nanoparticles volume fractions φ_1 and φ_2 on the temperature diffusion through the flow. As seen from these figures, it is found that the rise of φ_2, which represents the volume fraction of Cu or Ag nanoparticles, reduces heat diffusion. This result is compatible with that concluded by [48] in which it is found that the copper particles decrease the temperature of water. Contrariwise, one can see that the rise of $\varphi_1$improves heat transmission. This parameter is considered as a quantity of the random motion of the Al_2O_3 or CuO nanoparticles, which increases the temperature in the neighborhood of the BL as shown by Fig. 21. Naturally, the accidental or random motion of particles increases heat through liquid flow due to the evolution of friction force concerning those particles. Increasing the concentration of hybrid nanoparticles has two effects on temperature. On the one hand, it enhances heat transmission and thermal conductivity, which helps reduce temperatures. However, it also makes things more viscous, which can lead to a decrease in the rate of convective heat transfer and greater temperatures close to the surface. The equilibrium between these conflicting elements determines the final result. This result agrees with [54-56].

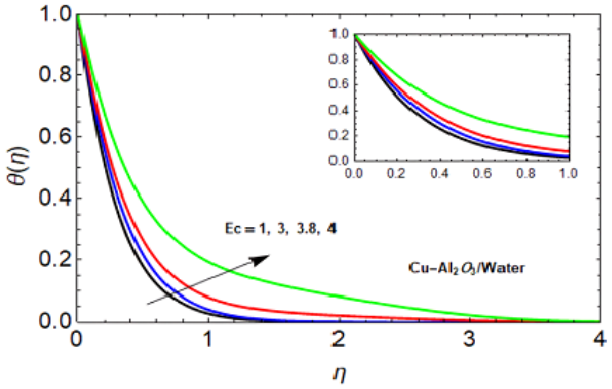

Fig. 10: Temperature profile $\theta(\eta)$ against η to show the influence of the Eckert numeral Ec in the case of Cu-Al_2O_3-water.

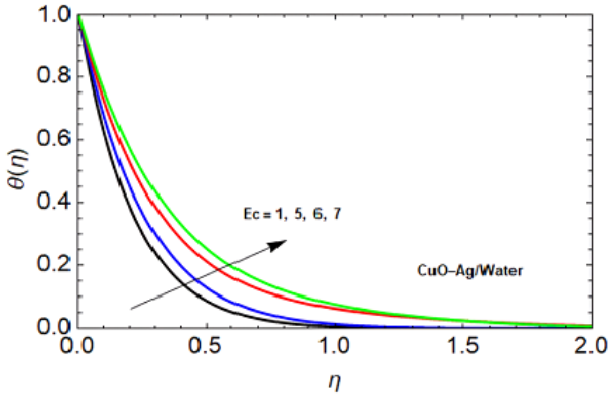

Fig. 11: Temperatu re profile $\theta(\eta)$ against η to show the influence of the Eckert numeral Ec in the case of CuO-Ag-water.

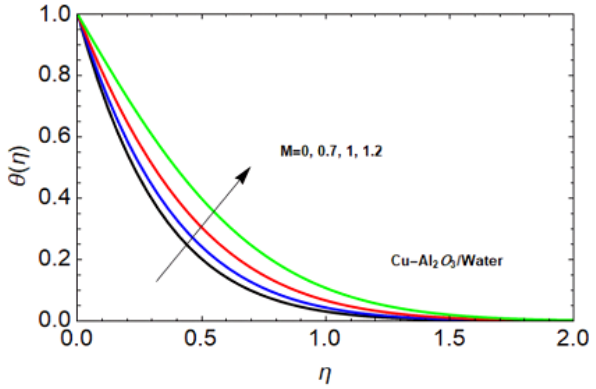

Fig. 12: Temperature distribution $\theta(\eta)$ versus η to show the influence of the magnetic coefficient M in the case of Cu-Al_2O_3-water.

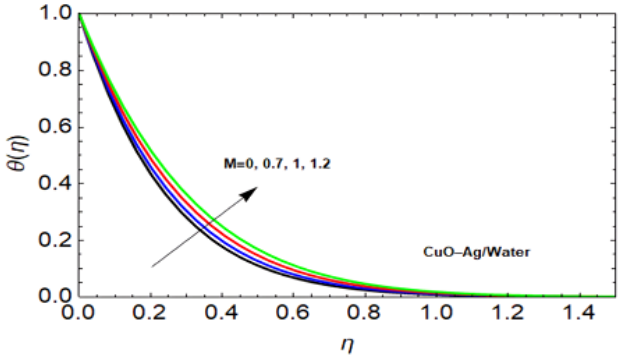

Fig. 13: Temperature profile $\theta(\eta)$ vs η to show the influence of the magnetic coefficient M in the case of CuO-Ag-water.

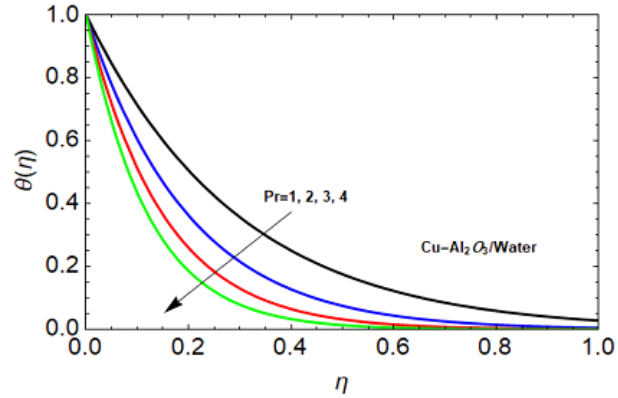

Fig. 14: Temperature profile $\theta(\eta)$ against η to display the influence of the Prandtl numeral Pr in the case of Cu-Al_2O_3-water.

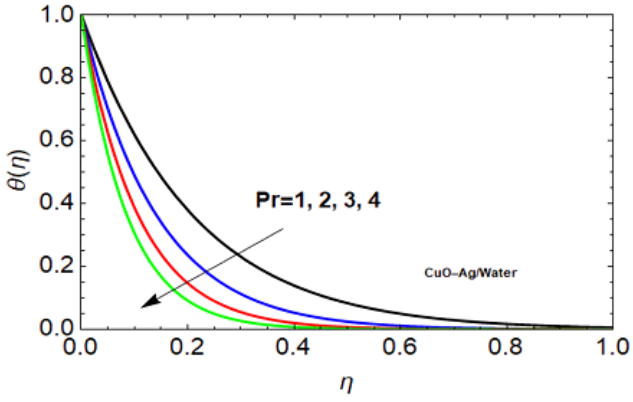

Fig. 15: Temperature profile $\theta(\eta)$ against η to display the effect of the Prandtl numeral Pr in the case of CuO-Ag-water.

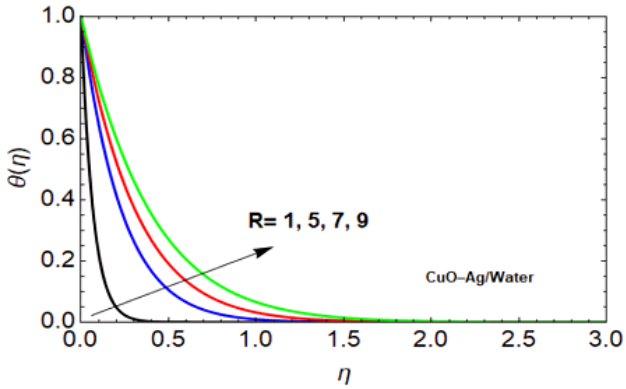

Fig. 16: Temperature distribution $\theta(\eta)$ vs η to display the effect of the radiation coefficient R in the case of Cu-Al_2O_3-water.

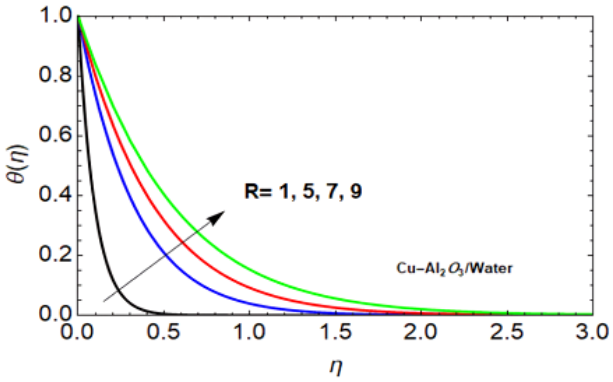

Fig. 17: Temperature distribution $\theta(\eta)$ vs η to display the effect of the radiation coefficient R in the case of CuO-Ag-water.

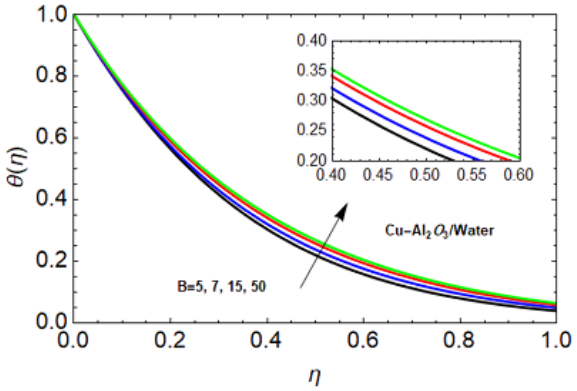

Fig. 18: Temperature profile $\theta(\eta)$ vs η to display the influence of the viscoelastic coefficient B in the case of Cu-Al_2O_3-water.

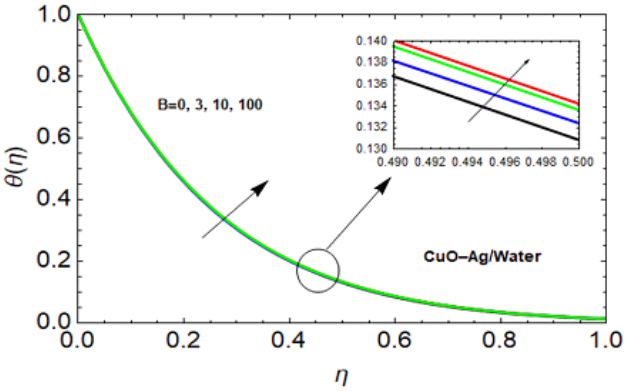

Fig. 19: Temperature profile $\theta(\eta)$ vs η to display the influence of the viscoelastic coefficient B in the case of CuO-Ag-water.

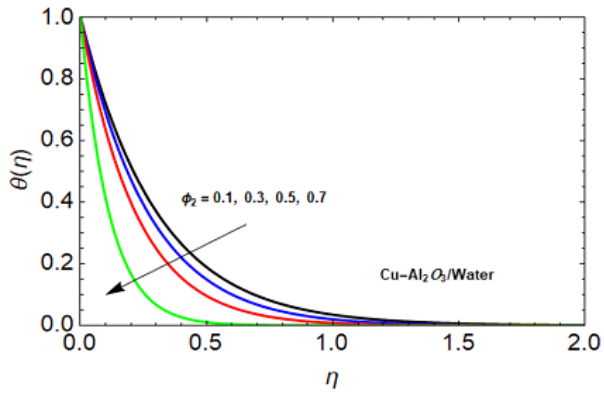

Fig. 20: Temperature profile $\theta(\eta)$ against η to display the effect of the volume fraction coefficient ϕ_2.

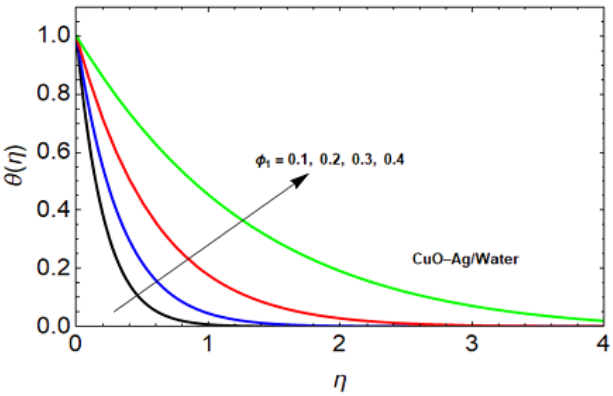

Fig. 21: Temperature profile $\theta(\eta)$ against η to show the impact of the volume fraction coefficient ϕ_1.

Skin Friction, and Nusselt Coefficients

Table 3 is designed to discuss the influences of the slip factor s on the skin friction parameter $f''(0)$ and compare its values with the previously concluded data of [55] and [56] to validate the current numerical accuracy. As attained in Table 1, there is a good agreement with the works of [55] and [56]. It is shown that the skin friction and Nusselt coefficients rise with the rise of s. This effect is opposite to that obtained previously on the speed $f'(\eta)$ and heat $\theta'(\eta)$ profiles.

Table 3 Skin friction and Nusselt coefficients compared with [55] and [56] when $B = \alpha = A = 0$ for different amounts of the slip factor s.

S	$f''(0)$			$\theta'(0)$		
	Waini [55]	Sparrow [56]	Present results	Waini [55]	Sparrow [56]	Present results
-2	0.4897	-	0.47581	0.00586	-	0.00588
-1	0.7605	0.756575	0.75657	0.1173	0.116 752	0.11687
-0.5	0.9697	0.969230	0.9692	0.2952	0.294 975	0.295005
0	-	-	0.8503	-	-	0.12942
0.5	-	-	0.78594	-	-	0.28383
1	-	-	0.78584	-	-	0.47681

5. Concluding Remarks

Maxwell hybrid nanofluid movement above a stretched surface with a stagnation point under the impacts of uniform normal magnetic strength, thermal radiation, and Joule heating is considered in the current analysis. The variation of speed and heat profiles has been illustrated. The innovation of the present examination arises from the participation of the hybrid nanoparticles Al2O3-Cu within the flow velocity and temperature utilizing the Maxwell model as a suitable non-Newtonian category. In applications such as electronics, heat exchangers, and automotive cooling systems, hybrid nanofluids' much higher thermal conductivity over base fluids results in improved heat dissipation and quicker cooling. The present model gives a comprehensive knowledge of how hybrid nanofluids behave in real-world applications under a variety of situations (magnetic fields, stretching surfaces, etc.) by incorporating not only heat transfer but also fluid dynamics (velocity profiles, boundary layer analysis). It is believed that this model has a significant applicable role in some engineering and industrial manufacturing mechanisms, like cooling of nuclear reactors, cooling of microelectronic devices by fans, wire drawing, polymer extrusion, and many engineering hydrodynamic applications. Moreover, the novel approach of the present study arises from the necessity of shedding light on the role of nanomaterials in the use of flow on stretching plates. As regular, proper similarity transforms have been demonstrated to convert a structure of PDEs that govern the profiles of velocity and heat to an ordinary one. This ordinary nonlinear system of equations has been analyzed numerically via RK-4 in combination with the shooting process. Graphical representations of the distributions are examined to identify the influences of the pertinent material parameters. The most pervasive outcomes concluded from this study are summarized as follows:

- The stagnation point represents a separate point between two regions of the hybrid nanofluid. Across this point, the effect of the MF on the velocity is reversed.
- Speed improves with the rise of the stagnation point value, the viscoelasticity factor, and the volume fractions of Al2O3 and CuO nanoparticles. On the contrary, the speed decays with the volume fractions of Cu and Ag nanoparticles.
- Heat transmission improves with the rise of all connected parameters except the Prandtl number and the volume fractions of Cu and Ag nanoparticles which decrease it.
- Hybrid nanoparticles volume fractions have a strong role in the impacts of other factors on both the speed and heat distributions.
- Skin friction and Nusselt coefficients have been numerically examined with different amounts of the slip coefficient and compared with previous works.

Acknowledgements

The author, Ahmed A Gaber, would like to thank the deanship of scientific research of Majmaah University for supporting this work under Project Number (R-2025-1518)

Future work

1. Examination of homogeneous and heterogeneous chemical reactions.
2. Illustration of a variety of heat sources.
3. Another classes of non-Newtonian fluids and hybrid nanoparticles could be discussed.
4. Examine how different hybrid nanoparticle volume fractions affect the thermal performance and energy efficiency.

Declaration of interest

There are no conflicts of interest declared by the authors.

Data Availability

All data produced or analyzed throughout this research are contained in this manuscript.

References

[1] Ali R.I., A review on nanofuid: preparation, stability, thermophysical properties, heat transfer characteristics and application, SN Applied Sciences, 2(10), 1636 (2020).

[2] Abu-Zeid M.A., Elhenawy Y., Bassyouni M., Majozi T., Toderas M., Al-Qabandi O.A., and Kishk S.S., Performance enhancement of flat-plate and parabolic trough solar collector using nanofluid for water heating application, Results in Engineering, 21, 101673 (2024).

[3] Hussain A., Dar M.N.R., Mujtaba A., Hussain F., Farooq N., and Hassan A.M., Slip effects on 3-D spinning dual-phase nanofluid flow over an exponentially stretching sheet with variable viscosity, Results in Engineering, 20, 1011387 (2023).

[4] Ullah Z., Abbas A., El-Zahar E.R., Seddek L.F., Akgul A., and Hassan A.M., Significance of thermal density and viscous dissipation on heat and mass transfer of chemically reactive nanofluid flow along stretching sheet under magnetic field, Results in Engineering, 20, 1011413 (2023).

[5] Bhatti M.M., Sait S.M., Ellahi R., Sheremet M.A., and Oztop H., Thermal analysis and entropy generation of magnetic Eyring-Powell nanofluid with viscous dissipation in a wavy asymmetric channel, International Journal of Numerical Methods for Heat and Fluid Flow, 33 (5), 1609-1636 (2022).

[6] Rashidi M.M., Mahariq I., Nazari M.A., Accouche O., and Bhatti M.M., Comprehensive review on energy analysis of shell and tube heat exchangers, Journal of Thermal Analysis and Calorimetry, 147(14), 12301–12311 (2022).

[7] Ali B., Jubair S., Fathima D., Akhter A., Rafique K., and Mahmood Z., MHD flow of nanofluid over moving slender needle with nanoparticles aggregation and viscous dissipation effects, Science Progress, 106(2), 1-24 (2023).

[8] Khadija R., Mahmood Z., Alqahtani H., and Sayed M.E., Various nanoparticle shapes and quadratic velocity impacts on entropy generation and MHD flow over a stretching sheet with Joule heating, Alexandria Engineering Journal, 71, 147–159 (2023).

[9] Adnan, and Ashraf W., Heat transfer mechanism in ternary nanofluid between parallel plates channel using modified Hamilton-Crossers model and thermal radiation effects, Geoenergy Science and Engineering, 225, 211732 (2023).

[10] Adnan, Rahman K.U. , Mahmood Z. , Khan S.U., Ali A., Li Z., and Tlili I., Enhanced thermal study in hybrid nanofluid flow in a channel motivated by graphene/Fe3O4 and Newtonian heating, Results in Engineering, 21, 101772 (2024).

[11] Moatimid G.M., Mohamed M.A.A., and Elagamy Kh., Heat and mass flux through a Reiner–Rivlin nanofluid flow past a spinning stretching disc: Cattaneo–Christov model, Scientific Reports, 12, 14468 (24 Pages) (2022).

[12] Ji-Huan He, Galal M. Moatimid, Mona A. A. Mohamed, Khaled Elagamy, A stretching cylindrical Carreau nanofluid border layer movement with motile microorganisms and variable thermal characteristics, International Journal of Modern Physics B, 38(17), 2450223 (2023).

[13] Moatimid G.M., Mohamed M.A.A., and Elagamy Kh., A Williamson nanofluid with motile microorganisms across a vertical exponentially stretching porous sheet with varying thermal characteristics, Special Topics and Reviews in Porous Media, 15(1), 67–98 (2024).

[14] Moatimid G.M., Mohamed M.A.A., and Elagamy Kh., Sutterby nanofluid flow with microorganisms around a curved expanding surface through a porous medium: Thermal diffusion and diffusion thermo impacts, Journal of Porous Media, 27, 19-48 (2024).

[15] Moatimid G.M., Elgazery N. S., Mohamed M.A.A., and Elagamy Kh., Bio-convection flow of Sutterby nanofluid with motile microbes on stretchable sheet: Exponentially varying viscosity, Journal of Applied and Computational Mechanics, 10(3), 488–502

(2024).

[16] Norzawary N.H.A., Bachok N., and Ali F.M., Stagnation point flow over a stretching/shrinking sheet in s carbon nanotubes with suction/injection effects, CFD Letters, 12(2), 106–114 (2020).

[17] Shah G., Rehman A., and Sheikh N., Heat transfer analysis over the boundary layer stagnation-point flow of couple stress fluid over an exponentially stretching sheet, American Journal in Applied Mathematics, 10, 100–105 (2022).

[18] Turkyilmazoglu M., Stagnation point flow and heat transfer over stretchable plates and cylinders with an oncoming flow: Exact solutions, Chemical Engineering Science, 238, 116596 (2021).

[19] Mahabaleshwar U.S., Maranna T., Mishra M., Hatami M., and Sunden B., Radiation effect on stagnation point flow of Casson nanofluid past a stretching plate/cylinder, Scientific Reports, 14, 1387 (2024).

[20] Devdas E., Numerical dual solution of stagnation point flow and melting heat transfer of Casson fluid due to stretching sheet, Journal of Emerging Technologies and Innovative Research, 9(9), e434–e454 (2022).

[21] Yousefi H., Mahmoudi M., and Ghodusinejad M.H., Modeling and sensitivity analysis of a supersonic inductive Magnetohydrodynamic (MHD) generator, Future Technology, 3(2), 1-10 (2024).

[22] Jiang C., Wang T., Zhu S., Yu G., Wu Z. and Luo E., A method to optimize the external magnetic field to suppress the end current in liquid metal Magnetohydrodynamic generators, Energy, 282, 128251 (2023).

[23] Bera T.K., A Magnetohydrodynamic (MHD) power generating system: a technical review, In IOP Conference Series: Materials Science and Engineering, 955(1), 012075 (2021).

[24] Aoki M., and Takeda M., Study on the effect of magnetic Field on Seawater electrolysis using a channel flow cell to simulate a linear-type seawater Magnetohydrodynamic power generator, Chemistry Letters, 51(5), 542-545 (2022).

[25] Domínguez-Lozoya J.C., Cuevas S., Domínguez D.R., Ávalos-Zúñiga R., and Ramos E., Laboratory characterization of a liquid metal MHD generator for ocean wave energy conversion, Sustainability, 13(9), 4641 (2021).

[26] Noureddine B., Fatima M., Salah A.M., and Said D., Magnetohydrodynamic (MHD) energy harvesting in reverse osmosis desalination plants, Journal of Electrical Systems, 20(3), 5675-5684 (2024).

[27] Moatimid G.M., Mohamed M.A.A., and Elagamy Kh., A motion of Jeffrey nanofluid in porous medium with motile microorganisms between two revolving stretching discs: Effect of Hall currents, Journal of Porous Media, 25(10), 83–101 (2022).

[28] Moatimid G.M., Elgazery N.S., Mohamed M.A.A., Elagamy Kh., Bio-convection flow of Sutterby nanofluid with motile microbes on stretchable sheet: Exponentially varying viscosity, Journal of Applied and Computational Mechanics, 10(3), 488–502 (2024).

[29] Anastasiadis Y., and Vlahakis N., Amodel for general relativistic Magnetohydrodynamic spine jets, Astronomy & Astrophysics (A&A), 688, A11 (16 Pages) (2024).

[30] Shang H., Wu J., and Zhang Q., Stability and optimal decay for the 3D Magnetohydrodynamic equations with only horizontal dissipation, Journal of Evolution Equations, 24, 12 (2024).

[31] Said B.O., Mebarek-Oudina F., and M. A. Medebber M.A., Magneto-hydro-convective nanofluid flow in porous square enclosure, Frontiers in Heat and Mass Transfer, Published: 30 October (2024). DOI: 10.32604/fhmt.2024.054164

[32] Dharmaiah G., Mebarek-Oudina F., Balamurugan K.S., and Vedavathi N., Numerical analysis of the magnetic dipole effect on a radiative ferromagnetic liquid flowing over a porous stretched sheet, Fluid Dynamics & Materials Processing, Published Online: 31 October (2023). DOI: 10.32604/fdmp.2023.030325

[33] Ramesh G.K., Gireesha B.J., Hayat T., and Alsaedi A., Stagnation point flow of Maxwell fluid towards a permeable surface in the presence of nanoparticles, Alexandria Engineering Journal, 55, 857-865 (2016).

[34] Ibrahim W. and Gizewu T., Thin film flow of tangent hyperbolic fluid with nonlinear mixed convection flow and entropy generation, Mathematical Problems in Engineering, Volume 2021, 4836434 (16 Pages) (2021).

[35] Ibrahim W., Magnetohydrodynamics (MHD) flow of a tangent hyperbolic fluid with nanoparticles past a stretching sheet with second order slip and convective boundary condition, Results in Physics, 7 3723–3731 (2017).

[36] Jamshed W., Nasir N.A.M., Isa S.S.P.M., Safdar R., Shahzad F., Nisar K.S., Eid M.R., Abdel Aty A. and Yahia I.S., Thermal growth in solar water pump using Prandtl–Eyring hybrid nanofluid: a solar energy Application, Scientific Reports, 11, 18704 (2021).

[37] Jamshed W., Nisar K. S., Ibrahim R. W., Shahzad F., and Eid M. R., Thermal expansion optimization in solar aircraft using tangent hyperbolic hybrid nanofluid: a solar thermal application, Journal of Materials Research and technology, 14, 985-1006 (2021).

[38] Fox R. W., McDonald A. T., and Pritchard P. J., Introduction to Fluid Mechanics, John Wiley & Sons, New York, Volume 7 (1985).

[39] Ho C. M., and Chen S. H., Unsteady Kutta Condition of Plunging Airfoil, in Unsteady Turbulent Shear Flows, Springer, Berlin (1981).

[40] Taylor G. I., The formation of emulsions in definable fields of flow, Proceedings of the Royal Society of London, Series A, Containing Papers of a Mathematical and Physical Character, 146(858), 501-523 (1943).

[41] Devi S.P.A., and Devi S.S.U., Numerical investigation of hydromagnetic hybrid $CuAl_2O_3$/water nanofluid flow over a permeable stretching sheet with suction, International Journal of Nonlinear Sciences and Numerical Simulation, 17, 249–257 (2016).

[42] Awaludin I.S., Ishak A., and Pop I., On the stability of MHD boundary layer flow over a stretching/shrinking wedge, Scientific Reports, 8, 13622 (2018).

[43] Tiwari R.K., and Das M.K., Heat transfer augmentation in a two-sided lid-driven differentially heated square cavity utilizing nanofluids, International Journal of Heat and Mass Transfer, 50, 2002–2018 (2007).

[44] Rehman K.U., Malik M.Y., Zahri M., and Tahir M.: Numerical analysis of MHD Casson Navier's slip nanofluid flow yield by rigid rotating disk, Results in Physics, 8, 744-751 (2008).
[45] Rohsenow W.M., Hartnett J.P., and Cho Y.I., Handbook of Heat Transfer, New York, McGraw-Hill (1998). [46] Fatunmbi E.O., and Okoya S.S., Heat transfer in boundary layer magneto-micropolar fluids with temperature-dependent material properties over a stretching sheet, Advances in Materials Science and Engineering, 2020, Article ID 5734979, 11 pages (2020).
[46] Ishak A., Thermal boundary layer flow over a stretching sheet in a micropolar fluid with radiation effect, Meccanica, 45, 367-373 (2010).
[47] https://extras.csc.fi/math/nag/mark21/pdf/D02/d02agf.pdf .
[48] Eldabe N.T.M., Ghaly A.Y., Mohamed M.A.A., and Mahmoud M.S.H., MHD boundary layer chemical reacting flow with heat transfer of Eyring–Powell nanofluid past a stretching sheet, Microsystem Technologies, 24, 4945–4953 (2018).
[49] Moatimid G.M., Mohamed M.A.A., and Elagamy Kh., A motion of Jeffrey nanofluid in porous medium with motile microorganisms between two revolving stretching discs: Effect of Hall currents, Journal of Porous Media, 25(10), 83–101 (2022).
[50] Hussain A., Malik M.Y., Salahuddin T., Rubal A., and Khan M., Effects of viscous dissipation on MHD tangent hyperbolic fluid over a nonlinear stretching sheet with convective boundary conditions, Results in Physics, 7, 3502-3509 (2017).
[51] Moatimid G.M., Mohamed M.A.A., and Elagamy Kh., A Casson nanofluid flow within the conical gap between rotating surfaces of a cone and a horizontal disc, Scientific Reports, 12, 1-21 (2022).
[52] Moatimid G.M., Mohamed M.A.A., and Elagamy Kh., Heat and mass flux through a Reiner-Rivlin nanofluid flow past a spinning stretching disc: Cattaneo–Christov model, Scientific Reports, 12, 14468 (2022).
[53] Gaber A. A., Tayel I. M. and Mostafa D. M., Analytical investigation for hybrid nanofuid flow near the stagnation point over a stretching sheet via modified adomian decomposition method, Modern Physics Letters B, Modern Physics Letters B.
[54] Sparrow E.M., Eckert E.R.G., and Minkowycz W.J., Transpiration cooling in a magneto-hydrodynamic stagnation-point flow, Applied Scientific Research, 11, 125–147 (1963).
[55] Waini I., Ishak A., Pop I., MHD flow and heat transfer of a hybrid nanofluid past a permeable stretching/shrinking wedge, Applied Mathematics and Mechanics, 41, 507–520 (2020).